Vol. 21, No. 1(2022) Mat2504
Revista Mexicana de Ingeniería Química

Corrosion inhibition of aluminum 2024-T3 in 3.5% NaCl by using *litchi chinensis* extract

Uso del extracto de *litchi chinensis* como inhibidor de la corrosión del aluminio 2024-T3 en 3.5% NaCl

N.J.Anzurez Valdez[1], R. Lopez-Sesenes[1], A.K. Larios-Gálvez[2], E. Vazquez-Velez[3], J. Uruchurtu-Chavarin[2], J.G. Gonzalez-Rodríguez[2*]

[1] *Universidad Autónoma del Estado de Morelos, Facultad de Ciencias Químicas e Ingeniería, Av. Universidad 1001, Col. Chamilpa, 62209-Cuernavaca, Morelos, México.*
[2] *Universidad Autónoma del Estado de Morelos, Centro de Inv. En Ingeniería y Ciencias Aplicadas, Av. Universidad 1001, Col. Chamilpa, 62209-Cuernavaca, Morelos, México.*
[3] *Universidad Nacional Autónoma de Mexico, Instituto de Ciencias Físicas, Av. Universidad s/n, Col. Chamilpa, 62209-Cuernavaca, Morelos, México.*

Received: June 8, 2021; Accepted: November 18, 2021

Abstract

The corrosion inhibition of AA2024-T3 Aluminium alloy in 3.5 % NaCl solution by using *litchi chinensis* seed ethanolic extract has been evaluated by using potentiodynamic polarization curves, linear polarization resistance and electrochemical impedance spectroscopy tests. Results have shown that the extract was a good corrosion inhibitor with an efficiency that increased with its concentration. Corrosion and passivation current density values were decreased indicating that the extract behaves as an anodic type of corrosion inhibitor. Inhibitor was adsorbed on to the metal surface in a combination of physical and chemical, dominated by a physical type of adsorption following a Langmuir adsorption isotherm. Corrosion rate was decreased due to the formation of a protective corrosion products layer which blocked further corrosion of metal by electrolyte.
Keywords: Aluminium, corrosion, sodium chloride, green inhibitor, *litchi chinensis*.

Resumen

La inhibición de la corrosión del aluminio AA2024-T3 en solución de 3.5% NaCl mediante el extracto etanólico de semillas de *litchi chinensis* ha sido evaluado mediante curvas de polarización potenciodinámicas, resistencia a la polarización lineal y espectroscopia por impedancia electroquímica. Los resultados mostraron que el extracto es un buen inhibidor cuya eficiencia se incrementa con su concentración. Las densidades de corriente de corrosión y de pasivación fueron reducidas con el extracto, por lo que el inhibidor se comporta como un inhibidor anódico. El inhibidor se adsorbe sobre la superficie del metal mediante una combinación de adsorción física y química dominado por el de tipo física de acuerdo a una isoterma de adsorción de Langmuir. La velocidad de corrosión disminuyó debido a la formación de una capa de productos de corrosión protectores los cuales bloquean la corrosión del metal por el electrolito.
Palabras clave: Aluminio, corrosión, cloruro de sodio, inhibidor verde, *litchi chinensis*.

* *Corresponding author. E-mail*: ggonzalez@uaem.mx
https://doi.org/10.24275/rmiq/Mat2504
ISSN:1665-2738, *issn-e*: 2395-8472

1 Introduction

The combination of good mechanical properties, low density, good thermal conductivity, low price and excellent corrosion resistance make aluminium and its alloys to be widely used in the cars manufacturing, aerospace, shipping industry, food handling and electronic devices industry (Martin *et al*., 2017; Anbarasi & and Divya, 2017; He *et al*., 2014).For instance, density for aluminium, carbon steel, stainless steel, copper and titanium, which are within the most widely used metals in the industry, are 2.7, 7.85, 8.02, 8.9 and 4.54 g/cm^3 respectively; similarly, thermal conductivity for the same metals are 205, 50, 15, 385 and 16 W/ m K. On the other side, corrosion resistance of metals and alloys depend of the environment, but aluminium and its alloys develop a layer of aluminium oxide on their surface which provides them a high corrosion resistance in many environments (Martin *et al*., 2017; Anbarasi & Divya, 2017; He *et al*., 2014). Due to these unique properties, AA2024-T3 aluminum alloy is extensively used in the aerospace and ship industry (Mohammadi *et al*., 2020). This alloy also shows good corrosion resistance when exposed to the atmosphere and many aqueous environments because of a resistive oxide layer, Al_2O_3, spontaneously formed when exposed to air or to the oxygen present in most of aqueous environments and passivates the alloy. However, some ions such as chlorides, present in the sea, can disrupt this protective layer, and thus, making necessary to protect aluminium alloy from corrosion. One of the most popular and efficient ways to fight corrosion of aluminium and its alloys is the use of corrosion inhibitors. Nowadays, there is a high need to look for applicable corrosion inhibitors and those that are economically viable and environmentally friendly. However, synthetic organic corrosion inhibitors and traditional inorganic corrosion inhibitors have restrictive environmental regulations due to their hazardous effects (Flamini *et al*., 2012). These environmental issues have called for replacing these compounds by naturally sourced from seeds, fruits, leaves, and flowers of plants that can inhibit corrosion of materials in corrosive media (Xhanari & Finsgar, 2019). Further, they are inexpensive, harmless, readily obtainable, and environmentally accommodative. In that sense, natural products are widely reported as corrosion inhibitors for aluminum and its alloys by several authors (Solmaz *et al*., 2008). Natural compounds efficiency as corrosion inhibitors depends on the chemical composition like polyphenols, fatty acids, anthocyanins, and protein (Pal & Das, 2020; Salinas-Solano *et al*., 2020). In the last decade, many extracts from natural products have been evaluated as green, non-toxic, environmentally friendly corrosion inhibitors (Popoola, 2019; Esquivel-López *et al*., 2019; Rani & Basu, 2012; Njoku *et al*., 2016; Fouda *et al*., 2009; Umoren *et al*., 2009; Ladha *et al*., 2017; Ramírez-Arreola *et al*., 2020; Gerengi, 2012; Kumpawat *et al*., 2012; Halambek *et al*., 2013; López-Hernández *et al*., 2018; Gerengi & Sahin, 2012) such as citric acid, Sansevieria trifasciata extract, exudate gum from Raphia hookeri, illicium verum, and so on. For instance, Kumpawat (Kumpawat *et al*., 2012) evaluated stem alkaloid extract of different varieties of Holy Basil as corrosion inhibition of aluminium in HCl solution, whereas Halambek *et al*. (2013) evaluated the ethanolic solution of Ocimum basilicum L. oil as corrosion inhibitor for aluminium in 0.5 M HCl using weight loss measurements, potentiodynamic polarization, and Electrochemical impedance spectroscopy (EIS) methods. Finally, Gerengi studied the influence of date palm (*Phoenix dactylifera* L.) fruit juice on 7075 type aluminium alloy (AA7075) in 3.5% NaCl solution by Tafel extrapolation and EIS (Gerengi & Sahin, 2012). It was found that PDL fruit juice acted as a slightly cathodic inhibitor, and inhibition efficiencies increased with the increase of PDL fruit juice concentration.

Lychee (*litchi chinensis* Sonn.) is a tropical and subtropical evergreen plant that belongs to the only species of the genus Litchi in the Sapindaceae family (Choi *et al*., 2017). The fruit is consumed as a fresh or processed product, whereas its seeds are mainly discarded as waste. Therefore, the seed extract can be used as a corrosion inhibitor since it contains compounds such as saponins, polyphenols, fatty acids, anthocyanins, amino acids, and volatile oils (Paliga *et al*., 2017; Saisavoey *et al*., 2018; Man *et al*., 2016). Recently, ethanolic extract of lychee seeds revealed the composition of twenty compounds a lignanoside, four methyl jasmonates, as well as fifteen flavonoids (Xiong *et al*., 2020; Dong *et al*., 2019). These compounds contain active functional groups to inhibit the metal corrosion (Liao *et al*., 2018). However, there are no reports about the corrosion inhibition effects of lychee seed extract on aluminum. Therefore, the objective of this research work is to evaluate the use of lychee seed extract as corrosion inhibitor for AA2024-T3 in 3.5 wt.% NaCl. To achieve this, antioxidants contained in lychee seeds will be extracted and added

at different concentrations to the NaCl solution where AA2024-T3 alloy is corroded at 25 ?C. Inhibitor effect will be evaluated by using electrochemical techniques, whereas corroded specimens will be analyzed with the aid of electronic microscopy to elucidate a corrosion mechanism.

2 Experimental procedure

2.1 *Extract of Lychee seed*

The lychee seeds were separated from the fruit, washed with tap water, and dried in a hot oven at 60 ° C. This temperature was used because it has been reported that the stability temperature of polyphenols is below 80 ° C (Volf *et al*., 2014). The most significant moisture loss from lychee seeds was on the first day. Subsequently, the seed weight was constant on the fifth day. After this time, seeds were ground using a blender machine to obtain a powder with a larger surface area to extract its components. Alcohol (70%) was used to extract the polar compounds from the seed powder. The lychee seed powder (35 g) was placed on a Soxhlet system with ethanol in a relationship of 1: 4 respectively. The system was refluxed during four hours, as a reported elsewhere (Dong *et al*., 2019). Then the seed powder was dried in an oven at 80 ° C. The powder weight lost was taken as the mass of antioxidants extracted and solubilized in ethanol. The yield of antioxidants extracted from the total mass was 4 %. The extract was used as a solution. On the other hand, a lychee seed extract aliquot (5 ml) was dried in a vacuum to eliminate the ethanol. The product was characterized by FTIR spectroscopy in a Bruker Tensor 27 FT-IR Spectrophotometer (Pike Miracle Single-Bounce ATR Cell).

2.2 *Testing solution*

As working electrolyte, a 3.5 (wt. %) NaCl solution at 25 ºC was used, which is the solution widely used in the literature to simulate sea water (Martin *et al*., 2017; Anbarasi & Divya, 2017; He *et al*., 2014), and was prepared with analytical grade reagents. These conditions were chosen because sea water, which contains the aggressive ion chloride, has an average temperature of 25 ºC. Lychee extract was added in to this solution at different concentrations.

2.3 *Testing material*

As testing material, AA2024-T3 aluminum alloy with a nominal chemical composition, in wt. %, 3.8-5.0 Cu, 0.2-1.2 Mg, 0.4-1.0 Mn, 0.5-1.2 Si and Al as balance was used. Cylindrical specimens with 6.00 mm in diameter and 10.00 mm in length were encapsulated in commercial polymeric resin. Specimens were ground down to 600 grade emery paper, washed and rinsed with acetone.

2.4 *Electrochemical techniques*

Different electrochemical techniques were used including potentiodynamic polarization curves, and electrochemical impedance spectroscopy (EIS) measurements. For this purpose, an open to air glass cell was used, for which a silver/silver chloride and a 3 mm diameter graphite rode were used as reference and auxiliary electrodes respectively. Before starting the tests, the open circuit potential value (OCP) was monitored and allowed to reach a stable value. Potentiodynamic polarization curves were started by polarizing the specimens 600 mV more cathodic than the free corrosion potential value, E_{corr} , to find both cathodic oxygen reduction and hydrogen evolution electrochemical reactions; after this, potential was scanned towards the anodic direction at a scan rate of 1 mV/s ending at a potential value 600 mV more anodic than E_{corr} to find the passive region. Corrosion current density values, I_{corr} were calculated by using the Tafel extrapolation method. Inhibitor efficiency, I.E., was calculated as follows:

$$I.E.(\%) = \frac{I_{corr2} - I_{corr1}}{I_{corr1}} \times 100 \qquad (1)$$

where I_{corr2} and I_{corr1} are the corrosion current density value in absence and presence of the inhibitor respectively. Finally, EIS measurements, in both, Nyquist and Bode formats, were carried out at the E_{corr} value by applying a signal ± 15 mV peak-to-peak in the frequency interval of 0.05 to 20,000 Hz. Specimens from these 24 hours long experiments were analysed in a low vacuum Scanning electronic microscope (SEM) whereas micro chemical elemental analysis was performed with an energy dispersive analyser (EDS) attached to it.

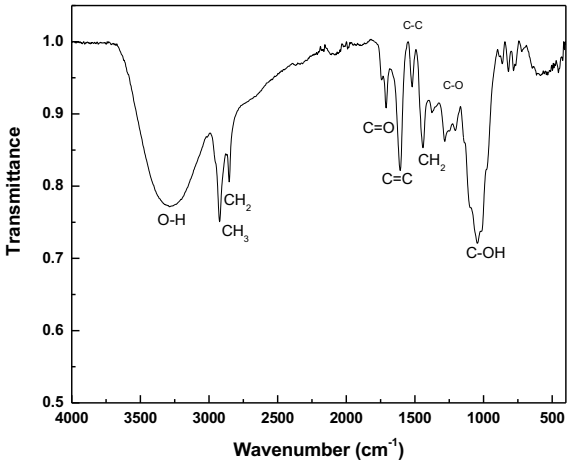

Fig. 1 FTIR spectrum of ethanolic lychee seed extract.

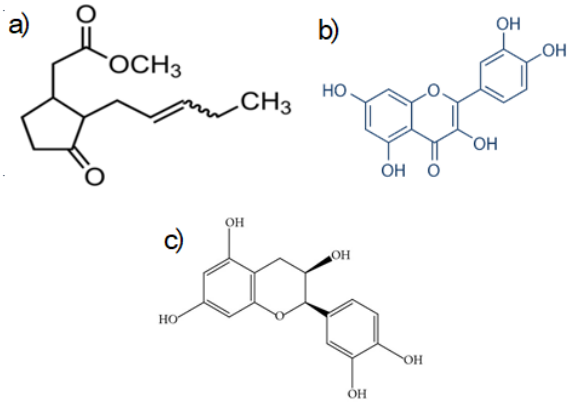

Fig. 2 Chemical structure of a) methyl jasmonate, b) quercetin and c) epicatechin identified in the lychee seed extract.

3 Results and discussion

3.1 Inhibitor characterization

FTIR spectrum of the lychee seed extract is given in Fig. 1. Dong *et al*. found twenty compounds in the ethanolic extract of lychee seed, which was separated by chromatography (HPLC) and characterized by 1H and 13C NMR RMN spectroscopy (Dong *et al*., 2019). They elucidated the molecule of each constituent and reported four new compounds and sixteen known compounds. The main components in the seed extract are methyl jasmonates, a flavonoid called quercetin, and epicatechin, with chemical structures as given in Fig. 2. In addition to this, Paliga *et al*. (Paliga *et al*., 2017) reported the presence of palmitic and oleic acids, with very similar structures as those shown

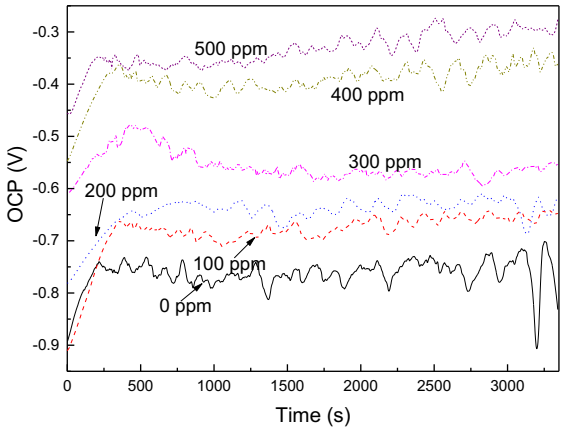

Fig. 3 Variation on the OCP value for AA2024-T3 aluminum alloy in 3.5% NaCl solution containing lychee seed extract.

in Fig. 2. The signals are in agreement with those reported in other studies (Popoola, 2019). Fig. 1 shows a broad signal of the O-H stretching vibration at 3293 cm^{-1}. The stretching vibration of C-H of the methyl and methylene group appears at 2925 and 2851 cm^{-1}. The signal for the C=O stretching vibration of the ester is at 1713 cm^{-1}, and at 1615 cm^{-1} appears a strong peak of the C=C vibration of unsaturated chains and benzene rings. Finally, the signal observed for the C-O stretch of the ether and ester group appears at 1235 cm^{-1}, whereas at 1042 cm^{-1} an intense peak for the C-O from the phenolic ring is observed.

3.2 Open circuit potential readings

The effect of the lychee seed extract concentration on the variation of the OCP value with time for AA2024-T3 aluminum alloy immersed in the 3.5 NaCl solution is depicted in Fig. 3. This figure shows that the OCP value shifts towards nobler values as the inhibitor concentration increases, finding the most active value in absence of inhibitor, due to its adsorption on the metal surface (Rahmouni *et al*., 2005). For each inhibitor concentration, during the beginning of the test, the OCP value starts to move in to the noble direction, this is because a film formed by the inhibitor and meal ions released during its dissolution starts to be built, until it reaches a steady state value due to the complete formation of a protective corrosion products film. However, regardless the inhibitor concentration, some oscillations in the OCP value once the steady state value has been reached due to the rupture and reformation of the corrosion products film formed by the inhibitor and the released metal ions during

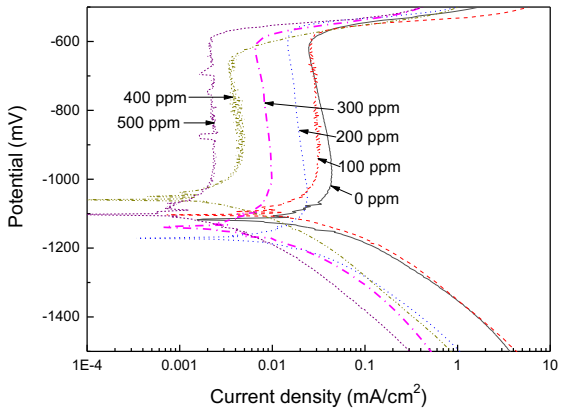

Fig. 4 Polarization curves for AA2024-T3 aluminum alloy immersed in 0.5 M NaCl in presence and absence of lychee seed extract at room temperature.

the metal dissolution process, indicating the film instability.

3.3 Potentiodynamic polarization curves

Polarization curves for AA2024-T3 aluminum alloy immersed in the 3.5 NaCl solution containing different concentrations of the lychee seed extract is shown in Fig. 4, where it can be seen that data display an active-passive behavior with a well-defined passive zone. In absence of inhibitor, this passive zone is due to the establishment of an Al_2O_3 layer on the alloy (Mohammadi *et al*., 2020; Flamini *et al*., 2012). In the open-to-air NaCl solution, the expected anodic reaction of Aluminum alloy is its dissolution:

$$Al \rightarrow Al^{3+} + 3e^{-} \tag{2}$$

whereas the main cathodic reaction is oxygen reduction:

$$\frac{1}{2}O_2 + 2H_2O + 3e^{-} \rightarrow 3OH - + \frac{1}{2}H_2 \tag{3}$$

with the formation of $Al(OH)_3$ according to:

$$Al^{3+} + 3OH^{-} \rightarrow Al(OH)_3 \tag{4}$$

which rapidly is transformed in to Al_2O_3 according to:

$$Al(OH)_3 \rightarrow Al_2O_3 \cdot 3H_2O \tag{5}$$

and this $Al_2O_3{\cdot}3H_2O$ is the responsible for the alloy passivation as long as there is oxygen present in the aqueous system.

Electrochemical parameters obtained from these curves are listed in table 1. This table shows that the E_{corr} value has an erratic behavior as the inhibitor is added, however, the corrosion current density value, I_{corr}, decreased as the inhibitor concentration increases, for nearly one order of magnitude, reaching its lowest value when 500 ppm of inhibitor were added. This decrease in the I_{corr} value with an increase in the inhibitor concentration is due to the adsorption of the lychee seed extract on the metal surface (Ngobiri *et al*., 2015; El Hamdani *et al*., 2015; Rajeswari *et al*., 2014; Ahamad *et al*., 2010; Verna *et al*., 2018). Inhibitor efficiency, I.E., behaved in the same fashion as the I_{corr} value did, increasing with the inhibitor concentration, reaching its highest value when 500 ppm of inhibitor were added in to the solution. In addition to this, the passive current density value, I_{pas}, decreased as the inhibitor concentration increased in the same way as the I_{corr} did. The pitting potential value, E_{pit}, practically remained unaffected by the inhibitor concentration, except at 400 ppm where it reached a slightly nobler value than that obtained in absence of inhibitor. Similar results were obtained by Singh (Singh *et al*., 2014) who evaluated a cationic *Coptis chinensis* root extract for 7075 aluminum alloy in 3.5 NaCl solution. In absence of inhibitor, the I_{corr} value they reported was 64 μA/cm^2, whereas for our alloy was 45.1?μA/cm^2; with the addition of 500 ppm of inhibitor, they obtained an I_{corr} value of 13 μA/cm^2, and an inhibitor efficiency of 79%, whereas in this research a value of 2.19 μA/cm^2 and an inhibitor efficiency of 95% were found. The main difference with 7075 aluminum alloy is the Zinc content, 5.9%, which is absent in the alloy used in this work. Similarly, Solmaz *et al*. (2008) evaluated citric acid as corrosion inhibitor for pure Al in 2.M NaCl, obtaining the highest efficiency, 87%, in a concentration of 1.0×10^{-5} M. On the other hand, the metal surface area covered by the inhibitor, ?, which is obtained by dividing the inhibitor efficiency value by 100, increased with the inhibitor concentration, which is evidence that the decrease in the corrosion current density is by the inhibitor adsorption on to the metal surface and to an increase in the area of the metal covered by it (Ahamad *et al*., 2010). Cathodic Tafel slope remained virtually the same as the inhibitor concentration increased, indicating that cathodic reactions such as oxygen reduction and hydrogen evolution were not affected, but we have seen a strong effect on the anodic side, and therefore we can say that lychee seed extract behaves basically as an anodic type of inhibitor.

Table 1 Electrochemical parameters obtained from polarization curves for AA2024-T3 aluminum alloy in 3.5% NaCl solution containing lychee seed extract.

C_{inh} (ppm)	E_{corr} (mV)	I_{corr} (mA/cm^2)	E_{pit} (mV)	I_{pas} (mA/cm^2)	β_c (mV/dec)	I.E. (%)	θ
0	-1120	4.51×10^{-2}	-611	4.8×10^{-2}	150	—	—
100	-1170	2.92×10^{-2}	-588	3.2×10^{-2}	160	35	0.35
200	-1100	2.1×10^{-2}	-595	2.4×10^{-2}	140	53	0.53
300	-1130	8.4×10^{-3}	-604	8.7×10^{-3}	150	81	0.81
400	-1060	4.42×10^{-3}	-662	4.8×10^{-3}	145	90	0.90
500	-1100	2.19×10^{-3}	-598	2.4×10^{-3}	145	95	0.95

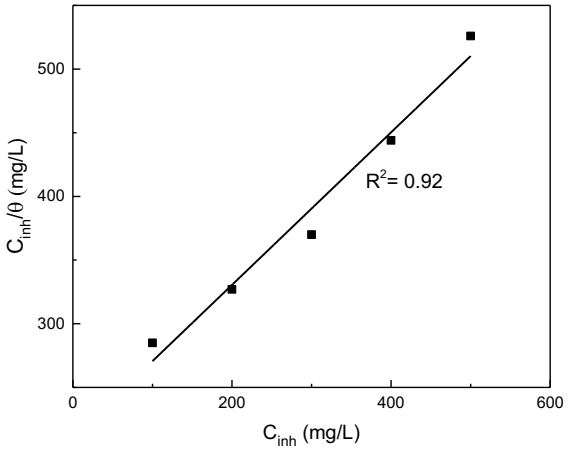

Fig. 5 Langmiur adsorption isotherm for AA2024-T3 aluminum alloy immersed in 0.5 M NaCl in presence and absence of lychee seed extract.

3.4 Adsorption isotherms

In order to elucidate more information the way that the lychee seed extract is adsorbed on to metal surface, it is necessary to use different adsorption isotherms such as Langmuir, Temkin and Frumkin ones. According to Fig. 5, results were fitted to the Langmuir type of adsorption isotherm (Ahamad *et al.*, 2010) which is given by:

$$\frac{C_{inh}}{\theta} = \frac{1}{K_{ads}} + C_{inh} \tag{6}$$

were the inhibitor concentration is represented by C_{inh}, K_{ads} is the adsorption constant = 3.12×10^{-2} L/mg.

Standard adsorption free energy, ΔG^0_{ads} and the adsorption constant, K_{ads}, are related through following expression:

$$\Delta G^0_{ads} = -RT \ln(10^6 K_{ads}) \tag{7}$$

where R is the universal gas constant, T is the absolute temperature.

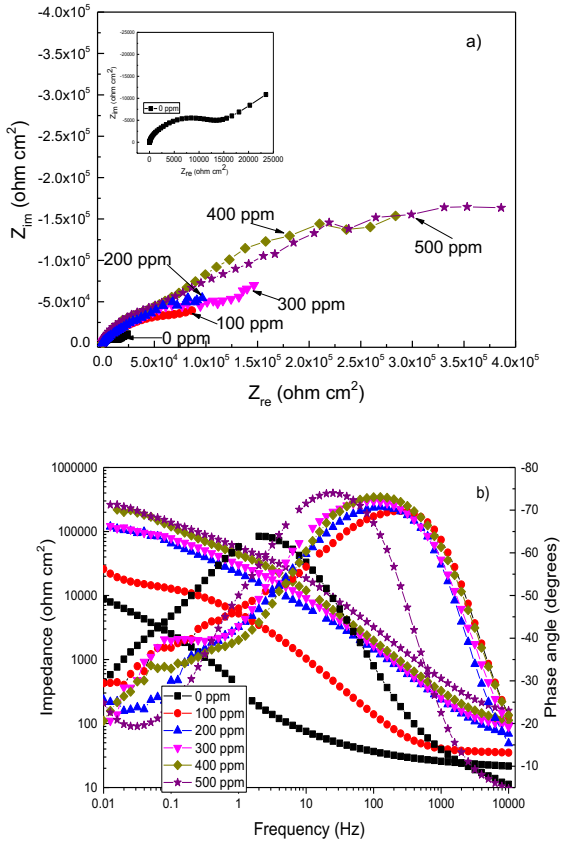

Fig. 6 Effect of lychee seed extract concentration in the a) Nyquist and b) Bode diagrams for AA2024-T3 aluminum alloy in 3.5% NaCl solution.

From data plotted in Fig. 6, a value obtained for ΔG^0_{ads} is -28.34 kJ mol^{-1}, which, according to literature (Ahamad *et al.*, 2010) if this value is lower than -20 kJ mol^{-1} there exists physical adsorption, whereas if this value is lower than -40 kJ mol^{-1} exists chemical adsorption; thus, a value of -28.34 kJ mol^{-1} is consistent with a mixture of a physical and chemical type of adsorption dominated by a physical, weak type of adsorption.

3.5 Electrochemical impedance spectroscopy measurements

EIS data in both Nyquist and Bode formats for AA2024-T3 aluminum alloy immersed in the 3.5 NaCl solution containing different concentrations of the lychee seed extract is shown in Fig. 6. In absence of inhibitor, Nyquist data describe a single depressed, capacitive loop at high and intermediate frequencies with its center at the real axis, followed for what looks like an unfinished second semicircle at lower frequency values, Fig. 6 a. Bode diagrams in the impedance-frequency format, Fig. 6 b, shows 2 different slopes in this case, which confirms the existence of two different time constants. Thus, it can be said that the high frequency semicircle is related to the electrochemical reactions taking place at the metal/corrosion products layer, due to the presence of an Al_2O_3 layer of corrosion products, whereas the low frequency loop represents the electrochemical reactions taking place at the metal/double electrochemical layer (Mohammadi *et al*., 2020; Flamini *et al*., 2012; Xhanari & Finsgar, M., 2019; Solmaz *et al*., 2008; Pal & Das, 2020). In presence of the lychee seed extract, Nyquist diagrams describe one depressed capacitive semicircle at high and intermediate frequency values followed by a second capacitive semicircle at lower frequencies. The diameters of both semicircles increased with the inhibitor concentration. As established above, the high frequency semicircle represents the electrochemical reactions taking place at the metal/corrosion products layer, whereas the low frequency loop represents the electrochemical reactions taking place at the metal/double electrochemical layer, and the corrosion products layer is due to the reaction between the inhibitor and freshly generated Al^{3+} ions. On the other hand, Bode diagrams in the phase angle-frequency format, Fig. 8 b, show a single peak in absence of inhibitor, but this peak is broadened as the inhibitor concentration increases and two overlapped peaks appeared at higher frequency values due to the presence of the protective layer formed between the inhibitor and released metal ions. The phase angle also increased as the inhibitor concentration increased, having a value of -62 degrees in absence of inhibitor down to -75 degrees when 500 ppm of inhibitor were added, which might be due to a decreases in the metal dissolution rate due to the addition of inhibitor.

It is frequent the use of electric circuits like the one shown in Fig. 7 to simulate the EIS response of a metal being corroded in presence or absence of an inhibitor.

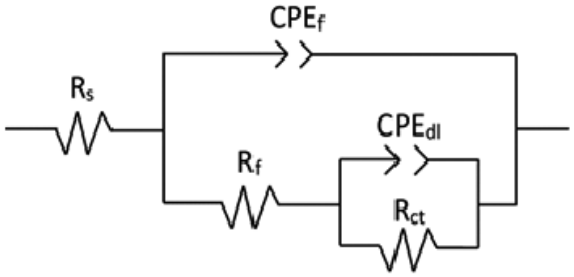

Fig. 7 Electric circuit used to simulate EIS data of AA2024-T3 aluminum alloy in 3.5% NaCl solution in presence of lychee seed extract.

In this figure, the electrolyte or solution resistance is represented by Rs, whereas the double electrochemical layer parameters such as charge transfer resistance and its capacitance are represented by R_{ct} and C_{dl} respectively; finally, the corrosion products layer parameters such as resistance and capacitance are represented by R_f and C_f; however, since the observed semicircles in the Nyquist diagrams are depressed due to surface heterogeneities due to its dissolution, ideal capacitances C_d and C_f are replaced by a constant phase elements, CPE_{dl} and CPE_f respectively. The impedance of a constant phase elements, Z, is given by:

$$Z_{CPE} = \frac{1}{Y(jw)^n} \tag{8}$$

where Y is the admittance, and n is related to the surface roughness and to the angle rotation of a pure capacitance. Obtained parameters used to simulate EIS data by using circuit shown in Fig. 10 are given in table 2. It can be seen that both charge transfer and film layer resistance values increased whereas the double electrochemical layer and film layer capacitance values decreased with increasing the lychee seed extract concentration. Singh (Singh *et al*. 2014) who evaluated a cationic *Coptis chinensis* root extract for 7075 aluminum alloy in 3.5 NaCl solution, reported Rct values of 4065 and 22072 ohm cm^2 at 0 and 500 ppm of inhibitor respectively (Solmaz *et al*. 2008), using citric acid as corrosion inhibitor for pure Al in 2.M NaCl reported value of 300 ohm cm^2 in absence of inhibitor and a maximum value of 2184 ohm cm^2, whereas in this work values of 6860 and 84854 ohm cm^2 at the same inhibitor concentrations are reported, which is very encouraging. Inhibitor efficiency, calculated as:

$$I.E.(\%) = \frac{R_{ct(inh)} - R_{ct(blank)}}{R_{ct(inh)}} \times 100 \tag{9}$$

Table 2 Parameters used to fit EIS data for for AA2024-T3 aluminum alloy in 3.5% NaCl solution containing lychee seed extract.

C_{inh} (ppm)	R_s (ohm cm^2)	C_{dl} (F cm^2)	n_{ct}	R_{ct} (ohm cm^2)	C_f (F cm^2)	n_f	R_f (ohm cm^2)	I.E. (%)
0	3.5	1.7×10^{-5}	0.79	6860	2.29×10^{-5}	0.52	14250	
100	3.2	4.1×10^{-6}	0.83	7025	4.38×10^{-5}	0.57	26844	5
200	3.3	2.41×10^{-6}	0.85	7995	1.18×10^{-6}	0.61	128587	15
300	3.4	1.08×10^{-6}	0.87	20875	1.12×10^{-6}	0.65	183586	67
400	3.5	7.8×10^{-7}	0.89	80265	3.16×10^{-6}	0.69	206858	91
500	3.6	3.3×10^{-7}	0.91	84854	1.12×10^{-6}	0.71	225863	93

where $R_{ct(blank)}$ and $R_{ct(inh)}$ are the charge transfer resistance values in the uninhibited and inhibited solution respectively, also increased with the inhibitor concentration. The increase in the R_{ct} value as the inhibitor concentration increased is due to its adsorption on the metal surface, whereas the decrease in the double layer capacitance, C_{dl}, is due to the organic inhibitor adsorption on to the metal surface and to the displacement of water molecules from the surface according to following:

$$Inh_{sol} + nH_2O_{ads} \rightarrow Inh_{ads} + nH_2O_{sol} \tag{10}$$

were Inh$_{sol}$ is the inhibitor into the solution, Inh$_{ads}$ is the adsorbed inhibitor on to the metal surface which have replaced n molecules of water adsorbed from the metal in to the solution; an alternative way to calculate double layer capacitance, C$_{dl}$, is as follows:

$$C_{dl} = \frac{\varepsilon \varepsilon_0 A}{\delta} \tag{11}$$

where?δ is the double layer thickness, ε is the double layer dielectric constant, ε_0 the vacuum electrical permittivity, and A the surface area. Thus, the adsorption of the inhibitor which has a lower dielectric constant value is the cause of the decrease in the capacitance value. On the other hand, the increase in the film layer resistance, R_f, is due to the increase in thickness of this film due to the reaction of the inhibitor with the released metallic ions during the alloy dissolution to form a compound which increases in thickness as more metal ions are released. Finally, values for parameter n gives a measure of the surface roughness due to the metal dissolution, taking values close to 1 when a low dissolution rate is taking place on the metal surface leading to a low surface roughness; on the other hand, values close to 0.5 are due to a high dissolution metal rate leading to a high surface roughness. Thus, n_{ct} values increased from 0.79 in absence of inhibitor due to a high dissolution rate to a value of 0.91 at the highest inhibitor concentration where the lowest metal dissolution rate was obtained and a lowest surface inhomogeneities due to the inhibitor adsorption as explained above.

3.6 Surface morphology analysis

It has been established above that the reduction in the dissolution rate of AA2024-T3 aluminum alloy immersed in the 3.5 NaCl solution is due to the adsorption of the lychee seed extract on to its surface to form a layer of protective corrosion products. In order to determine this, corroded specimens in absence and presence of inhibitor were analyzed in the scanning electronic microscope (SEM) and the micrographs are presented in Fig. 8. In absence of inhibitor or in concentrations lower than 200 ppm, Figs. 8 a, b and c, the metal surface is not fully covered by the corrosion products layer and some forms of localized type of corrosion such as pits were present. At a concentration of 300 ppm, Fig. 8 d, a layer of corrosion products covers almost completely the metal surface, however, such a layer presents a high number of cracks which serve as pathways for the corrosive environment penetrate though them and attack the underlying metal. Some pits were observed also. As the inhibitor concentration increased, Figs. 8 e and f) the layer of corrosion products covers a much higher surface metal area, the number of cracks decreases dramatically at 400 ppm, whereas at 500 ppm, a smooth, almost defects free film which protects the metal was observed.

3.7 Corrosion mechanism

To better explain the corrosion inhibition process and mechanism of the antioxidant constituents in the lychee seed extract on the steel surface, a schematic diagram of their adsorption is shown in Fig. 9. The compounds have a strong electron-donating and chelating capacity with metals, giving the extract ability to inhibit metal corrosion. This chemisorption is preferable by an electronic interaction between

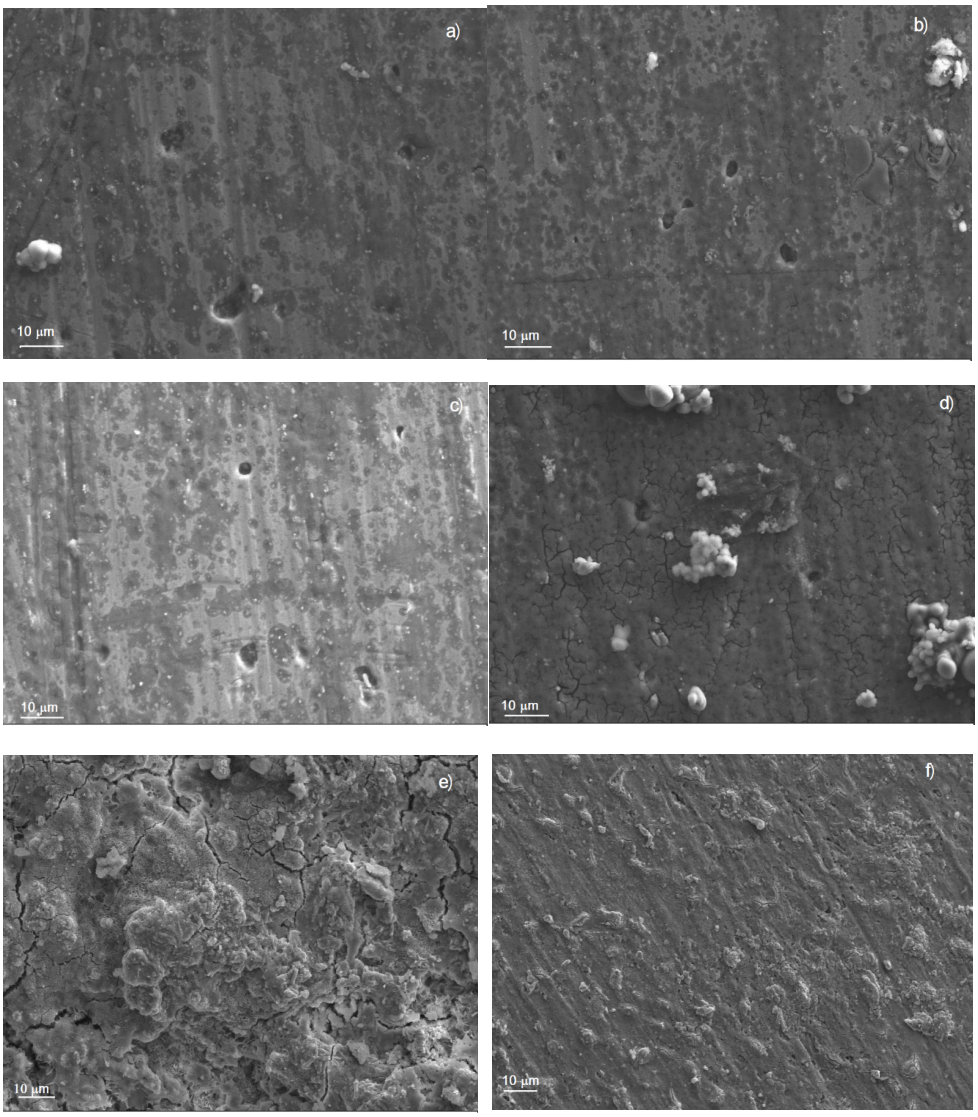

Fig. 8 SEM micrographs of AA2024-T3 aluminum alloy corroded in 3.5% NaCl solution containing a) 0, b) 100, c) 200, d) 300, e) 400 and e) 500 ppm of lychee seed extract.

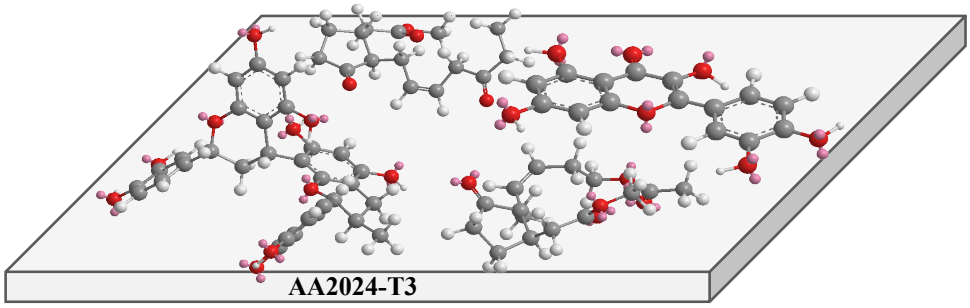

Fig. 9 Chemisorption of the antioxidant constituents in the lychee seed extract.

the unshared pairs electrons (pink) from heteroatoms (red) and the π orbitals bond (dotted line) from the molecules and the benzene rings with the d orbitals on the metallic surface until the formation of a very rigid barrier of molecules. As it was mentioned above in Fig. 2, the lychee see extract contains in its structure compound such as Methyl Jasmonate, Quercitin and Epicatchin, all of them contain aromatic rings linked with Carbon ring containing mainly hydroxyl groups and oxygen. The oxygen and OH^- groups are chemically adsorbed over the metal surface through adsorption due to a donor-acceptor interaction between them and the metallic surface. The free positions in the π orbital in Al, Mg and Cu, allows the donation of electrons to the Oxygen and Hydrogen molecules allowing the formation of a barrier that blocks the exchange electrons between the anodic and cathodic sites forming a protective passive layer composed mainly of Al_2O_3, $Al(OH)_3$ and AlO(OH) [34]. Typically, the AA2024-T3 shows two-time constants with in presence of inhibitor where the formed at low frequencies is attributed to the absorption of the inhibitor over the metal surface that blocks the cathodic sites which contain copper and magnesium particles, reducing the molecular interaction with the metal surface.

Conclusions

A study on the use of the ethanolic extract of lychee seeds as corrosion inhibitor for AA2024-T3 aluminum alloy in 3.5% NaCl solution has been performed. Lychee seed extract resulted a good corrosion inhibitor with an efficiency which increased with its concentration. Highest inhibitor efficiency value, higher than 90%, was reached with the addition of 500 ppm. Polarization curves showed that this extract behaves basically as an anodic type of inhibitor Corrosion current density value was decreased for more than on order of magnitude, since it was decreased from 4.51×10^{-2} in the uninhibited solution, down to 2.19×10^{-3} mA/cm^2. In addition to this, passive film properties were improved since the passive current density value was decreased from 4.8×10^{-2} to 2.4×10^{-3} mA/cm^2 and its resistance increased from 8.4×10^4 to 2.2×10^5 ohm cm^2. The pitting potential value remained practically unaltered by the addition of the inhibitor, fluctuating around a value of -600 mV. Extract was adsorbed on to the metal surface following a Langmuir type of adsorption isotherm with a Gibbs free energy value of -28.34 kJ mol^{-1} in a weak physical type of adsorption. Morphological analysis of corroded surfaces indicated the formation of protective corrosion products on to the metal surface protecting it from the corrosive attack. In absence of inhibitor or lower concentrations than 300 ppm, the film formed by the inhibitor does not cover completely the metal surface or it presents numerous defects such as porous and micro cracks. At inhibitor concentrations of 400 and 500 ppm, the film-formed inhibitor is much more compact with a lower number of porous or micro cracks. A mechanism is given for which the lychee seeds extract compounds interact with metal to protect it from corrosion.

References

Ahamad, I., Prasad, R. and Quraishi, M.A. (2010). Adsorption and inhibitive properties of some new Mannich bases of Isatin derivatives on corrosion of mild steel in acidic media. *Corrosion Science 52*, 1472-1481. https://doi.org/10.1016/j.corsci.2010.01.015

Anbarasi, M.C. and Divya, G. (2017). A green approach to corrosion inhibition of aluminium in acid medium using azwain seed extract. *Materials Today 4*, 5190-5200. https://doi.org/10.1016/j.matpr.2017.05.026

Choi, S.A., Lee, J.E., Kyung, M.J., Young, J.H., Oh, J.B. and Whang, W.K. (2017). Anti-diabetic functional food with wasted litchi seed and standard of quality control. *Applied Biology Chemistry 60*, 197-204. https://doi.org/10.1007/s13765-017-0269-9.

Dong, X., Huang, Y., Wanga, Y. and He, X. (2019). Anti-inflammatory and antioxidant jasmonates and flavonoids from lychee seeds. *Journal of Functional Foods 54*, 74-80. https://doi.org/10.1016/j.jff.2018.12.040

El Hamdani, N., Fdil, R., Tourabi, M., Jama, C. and Bentiss, F. (2015). Alkaloids extract of *Retama monosperma (L.) Boiss*. seeds used as novel eco-friendly inhibitor for carbon steel corrosion in 1 M HCl solution: Electrochemical and surface studies. *Applied Surface Science 357*, 1294-1305. https://doi.org/10.1016/j.apsusc.2015.09.159

Esquivel-López, A., Cuevas-Arteaga, C., & Valladares-Cisneros, M. (2019). Study of the corrosion inhibition of copper in synthetic seawater by Equisetum arvense as green corrosion inhibitor. *Revista Mexicana de Ingeniería Química 19(2)*, 603-616. https://doi.org/10.24275/rmiq/Mat629

Flamini, D., Trueba, M. and Trasatti, S. (2012). Aniline-based silane as a primer for corrosion inhibition of aluminum. *Progress in Organic Coatings 74*, 302-309. https://doi.org/10.1016/j.porgcoat.2011.11.011

Fouda, A.S., Al-Sarawy, A.A., Ahmed, F.S. and El-Abbasy, H.M. (2009). Corrosion inhibition of aluminium 6063 using some pharmaceutical compounds. *Protion of Metals. Physicas and Chemistry Surfaces 45*, 635-643. https://doi.org/10.1134/S2070205109050244

Gerengi, H. and Sahin, H.I. (2012). Schinopsis lorentzii extract as a green corrosion inhibitor for low carbon steel in 1 M HCl solution. *Industrial and Engineering Chemistry Research 51*, 780-787. https://doi.org/10.1021/ie201776q

Gerengi, H. (2012). Anticorrosive properties of date palm (*Phoenix dactylifera* L.) fruit juice on 7075 type aluminum alloy in 3.5% NaCl solution. *Industrial and Engineering Chemistry Research 51*, 12835. https://doi.org/10.1021/ie301771u

Halambek, J., Zutinic, A. and Berkovic, K. (2013). Ocimum basilicum L. oil as corrosion inhibitor for aluminium in hydrochloric acid solution. *International Journal of Electrochemical Science 8*, 11201-11214.

He, X., Jiang, Y., Li, C., Wang, W., Hou, B. and Wu, L. (2014). Inhibition properties and adsorption behavior of imidazole and 2-phenyl-2-imidazoline on AA5052 in 1.0 M HCl solution. *Corrosion Science 83*,124-136. https://doi.org/10.1016/j.corsci.2014.02.004

Kumpawat, N., Chaturvedi, A. and Upadhyay, R.K. (2012). Study on corrosion inhibition efficiency of stem alkaloid extract of different varieties of holy basil on aluminium in HCl solution. *Journal of the Korean Chemical Society 56*, 401-405. http://dx.doi.org/10.5012/jkcs.2012.56.4.401

Ladha, D.G., Shah, N.K., Ghelichkha, Z., Obot, I.B., Dehkharghani, F.K., Yao, J.Z. and Macdonald, D.D. (2017). Experimental and computational evaluation of illicium verum as a novel eco-friendly corrosion inhibitor for aluminium. *Materials and Corrosion 69*, 1-15. https://doi.org/10.1002/maco.201709581

Liao, L.L., Mo, S., Luo, H.Q. and Li. N.B. (2018). Corrosion protection for mild steel by extract from the waste of lychee fruit in HCl solution: Experimental and theoretical studies. *Journal of Colloid and Interfaces Science 520*, 41-49. https://doi.org/10.1016/j.jcis.2018.02.071

López-Hernández, L., Calderón-Oliver, M., Soriano-Santos, J., Severiano-Pérez, P., Escalona-Buendía, H., & Ponce-Alquicira, E. (2018). Development and antioxidant stability of edible films supplemented with a tamarind seed extract. *Revista Mexicana de Ingeniería Química 17(3)*, 975-987. https://doi.org/10.24275/uam/izt/dcbi/revmexingquim/2018v17n3/Lopez

Man, S., Ma, J., Wang, C.X., Li, Y., Gao, W.Y. and Lu, F.P. (2016). Chemical composition and hypoglycaemic effect of polyphenol extracts from *litchi chinensis* seeds. *Journal of Functional Foods 22*, 313-324. https://doi.org/10.1016/j.jff.2016.01.032.

Martin, J.H., Yahata, B.D. and Hundley, J.M. (2017). 3D printing of high-strength aluminium alloys. *Nature 549*, 365-379. https://doi.org/10.1038/nature23894

Mohammadi, I., Shahrabi, T., Mahdavian, M., and Izadi, M. (2020) Sodium diethyldithiocarbamate as a novel corrosion inhibitor to mitigate corrosion of 2024-T3 aluminum alloy in 3.5 wt% NaCl solution. *Journal of Molecular Liquids 307*, 112965. https://doi.org/10.1016/j.molliq.2020.112965

Ngobiri, N.C., Oguzie, E.E., Li, Y., Liu, L., Oforka, N.C. and Akaranta, O. (2015). Eco-friendly corrosion inhibition of pipeline steel using *Brassica oleracea. International Journal of*

Corrosion 2015, 9 pages. https://doi.org/10.1155/2015/404139

Njoku, D.I., Ukaga, I., Ikenna, O.B., Oguzie, E.E., Oguzie, K.L. and Ibisi, N. (2016). Natural products for materials protection: corrosion protection of aluminium in hydrochlorica cid by Kola nitida extract. *Journal of Molecular Liquids 219*, 417-424. https://doi.org/10.1016/j.molliq.2016.03.049

Pal, A. and Das, C. (2020). A novel use of solid waste extract from tea factory as corrosion inhibitor in acidic media on boiler quality steel. *Industrial Crops and Products 151*, 112468. doi: 10.1016/j.indcrop.2020.112468

Paliga, M., Novello, Z., Dallago, R.M., Scapinello, J., Dal Magro, J., Di Luccio, M., Tres, M.V. and Oliveira, J.V. (2017). Extraction, chemical characterization and antioxidant activity of *litchi chinensis* Sonn and Avena sativa L. seeds extracts obtained from pressurized n-butane. *Journal of Food Science and Technology 54*, 846-851. https://doi.org/10.1007/s13197-016-2485-4.

Popoola, L.T., 2019. Progress on pharmaceutical drugs, plant extracts and ionic liquids as corrosion inhibitors. *Heliyon 5*, e 01143. https://doi.org/10.1016/j.heliyon.2019.e01143

Rahmouni, K., Keddam, M., Srhiri, A. and Takenouti, H. (2005). Corrosion of copper in 3% NaCl solution polluted by sulphide ions. *Corrosion Science 47*, 3249-3266. https://doi.org/10.1016/j.corsci.2005.06.017

Rajeswari, V., Kesavan, D., Gopiraman, M., Viswanathamurthi, P., Poonkuzhali, K. and Palvannan, T. (2014). Corrosion inhibition of *Eleusine aegyptiaca* and *Croton rottleri leaf* extracts on cast iron surface in 1 M HCl medium. *Applied Surface Science 314*, 537-545. https://doi.org/10.1016/j.apsusc.2014.07.017

Ramírez-Arreola, D., Aranda-García, F., Sedano de la Rosa, C., Camacho-Vidrio, A., & Silva, R. (2020). Corrosion behavior of steel reinforcement bars embedded in concrete with sugar cane bagasse ash. *Revista Mexicana de Ingeniería Química 19(Sup. 1)*, 469-481. https://doi.org/10.24275/rmiq/Mat1651

Rani, B. E. A. and Basu, B. B. J. (2012). Green inhibitors for corrosion protection of metals and alloys: An overview. *International Journal of Corrosion 2012*, 380217. https://doi.org/10.1155/2012/380217

Saisavoey, T., Sangtanoo, P., Reamtong, O. and Karnchanatat, A. (2018). Anti-inflammatory effects of lychee (*litchi chinensis* Sonn.) seed peptide hydrolysate on RAW 264.7 macrophage cells. *Food Biotechnology 32*, 79-94. https://doi.org/10.1080/08905436.2018.1443821.

Salinas-Solano, G., Porcayo-Calderon, J., Martinez de la Escalera, L. M., Canto, J., Casales-Diaz, M., Sotelo-Mazon, O. and Martinez-Gomez, L. (2018). Development and evaluation of a green corrosion inhibitor based on rice bran oil obtained from agro-industrial waste. *Industrial Crops and Products 119*, 111-124. doi: 10.1016/j.indcrop.2018.04.009

Solmaz, R., Kardaş, G., Yazici, B. and Erbil, M. (2008). Citric acid as natural corrosion inhibitor for aluminium protection. *Corrosion Engineering Science and Technology 43*, 186-191. https://doi.org/10.1179/174327807X214770

Umoren, S.A., Obot, I.B., Ebenso, E.E., and Obi-Egbedi, N.O. (2009). The Inhibition of aluminium corrosion in hydrochloric acid solution by exudate gum from *Raphia hookeri*. *Desalination 247*, 561-572. https://doi.org/10.1016/j.desal.2008.09.005

Verna, C., Olasunkanmi, L.O., Ebenso, E.E. and Quraishi, M.A. (2018). Adsorption characteristics of Green 5-arylaminomethylene pyrimidine-2,4,6-triones on mild Steel Surface in acidic medium: Experimental and computational approach. *Results in Physics 8*, 657-670. https://doi.org/10.1016/j.rinp.2018.01.008

Volf, I., Ignat, I., Neamtu, M. and Popa, V.I. (2014) Thermal stability, antioxidant activity, and photo-oxidation of natural polyphenols. *Chemical Papers 68*, 121-129. https://10.2478/s11696-013-0417-6

Xhanari, K. and Finsgar, M. (2019). Organic corrosion inhibitors for aluminum and its alloys in chloride and alkaline solutions: A review. *Arabian Journal of Chemistry 12*, 4646-4663. http://dx.doi.org/10.1016/j.arabjc.2016.08.009

Xiong, R., Wang, X.L., Wu, J.M., Tang, Y., Qiu, W.Q., Shen, X., Teng, J.F., Pan, R., Zhao, Y., Yu, L., Liu, J., Chen, H.X., Qin, D.L. and Yud, C.L. (2020). An-Guo Wua. Polyphenols isolated from lychee seed inhibit Alzheimer's disease-associated Tau through improving insulin resistance via the IRS-1/PI3K/Akt/GSK-3β pathway. *Journal of Ethnopharmacology 251*, 112548. https://doi.org/10.1016/j.jep.2020.112548.